Supplementary Material of "Self-Assembly of Chiral Tubules"

Shengfeng Cheng* and Mark J. Stevens†

Sandia National Laboratories, Albuquerque, NM 87185, USA

* Present address: Department of Physics, Virginia Polytechnic Institute and State University, Blacksburg, Virginia 24061, USA; chengsf@vt.edu

† msteve@sandia.gov

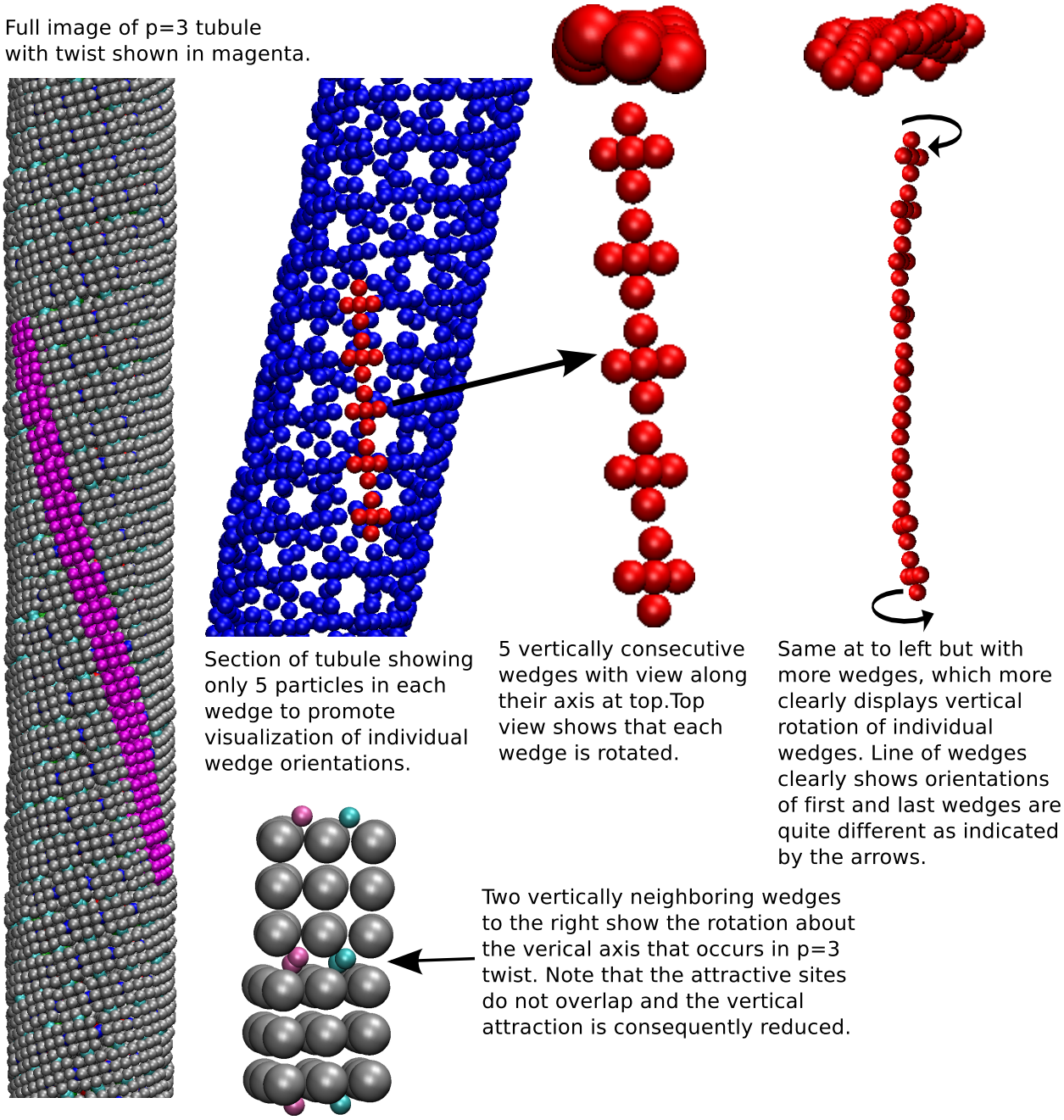

FIG. S1. An equilibrated 13_3 tubule of M_0 monomers with twisted protofilaments shows the rotation of wedges along a protofilament.

Using a 13_3 tubule of M_0 monomers as an example, Fig. S1 illustrates the limits of twist deformation of protofilaments when the helicity of a tubule does not match the the chirality of monomers. Because of the curvature of a tubule surface, a twisted protofilament has to curl around the central axis of the tubule, which in turn requires the rotation of wedge monomers along the protofilament and introduces an offset between the vertical binding

sites between two stacking neighboring wedges. If the required offset is too large, then the tubule will have a much higher energy than the one with helicity that matches the chirality of monomers, and the tubule will be energetically unfavored. Therefore, the key to suppress the rotation of wedges and thus the twist of protofilaments is to have a large A_V.

Equation (1) of the main text describes the twist deformation of protofilaments for all tubules built from any monomers that we have studied. One more example is included in Fig. S2 for tubules formed by M_2^{LK} monomers. In general, it is expected that Eq. (1) of the main text is applicable to all tubular structure made out of identical discrete building blocks.

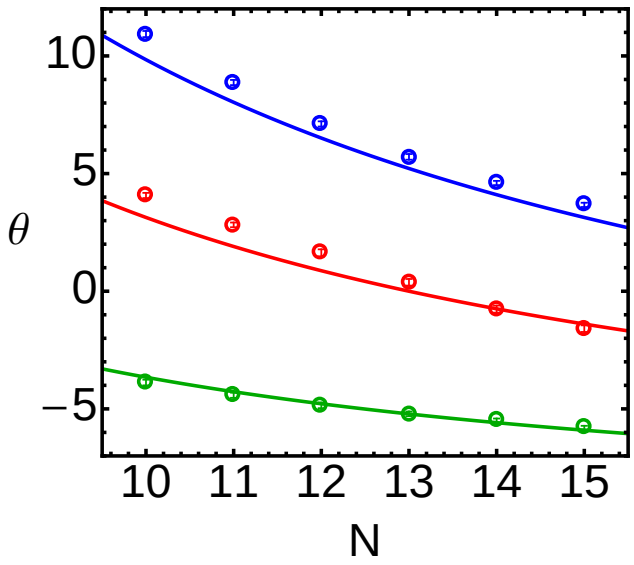

FIG. S2. The twist angle θ of protofilaments in tubules formed by M_2^{LK} monomers and with various number (N) of protofilaments and pitches: $p = 2$ (red), $p = 1$ (green), and $p = 3$ (blue) at $A_L = 3.0$ and $A_V = 6.3$. Symbols are simulation results with error bars comparable or smaller than the symbol size. Lines represent the corresponding predictions of Eq. (1) of the main text with $h = 3\sigma$ and $w = 2.53\sigma$.

We study the effects on the tubule twist deformation of both lateral and vertical binding interactions. One set of results is included in Fig. S3, which shows that the twist angle θ is insensitive to either A_L or A_V. This is not surprising, because θ is mainly determined by the geometric features of the building blocks, as expressed in Eq. (1) of the main text. However, the small changes of θ with A_L or A_V are still noteworthy. On the one hand, θ slightly decreases as A_V is increased while A_L is fixed, indicating that the twist deformation

is slightly reduced at a larger A_V. This trend can be understood on the basis that a large A_V makes the protofilaments stiffer and helps reduce the offset between the vertical binding sites of two stacking wedges in a protofilament (see Fig. S1), and a smaller offset leads to a more gently twisted protofilament and thus a smaller twist angle. On the other hand, θ essentially remains unchanged as A_L is varied at a small fixed A_V, or increases slowly with an increasing A_L at a large fixed A_V, which indicates that the twist deformation is slightly enhanced with a large A_L. The underlying physics is that a larger A_L implies a stronger adhesion between neighboring protofilaments, which favors a twisted packing of protofilaments. The similar trends in θ vs. A_L and A_V were observed for all tubules that we have built with our monomers (achiral/chiral, with/without lock-and-key vertical binding).

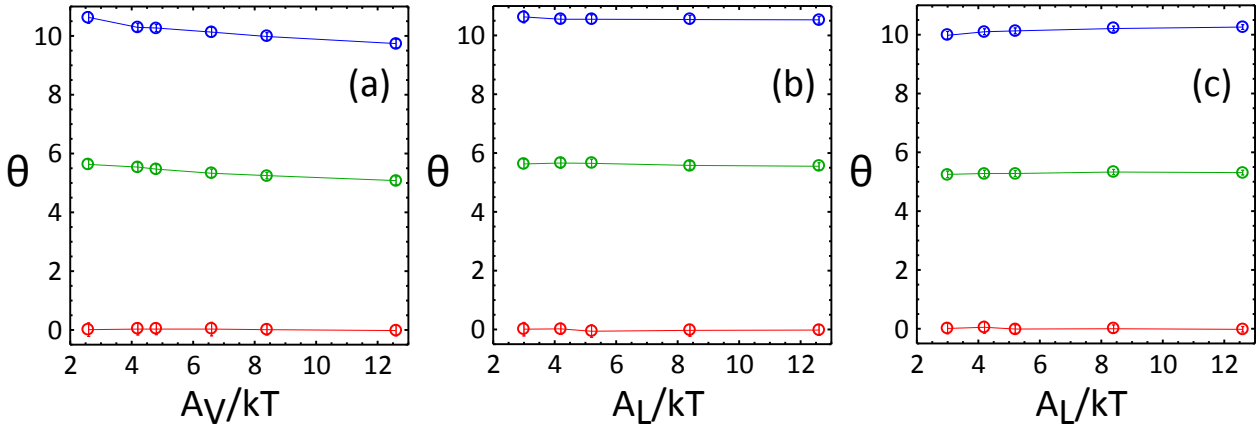

FIG. S3. θ vs. interaction strength: (a) $A_L = 3.0$ and A_V is varied; (b) $A_V = 2.6$ and A_L is varied; (c) $A_V = 8.4$ and A_L is varied. Data are for 13_p tubules built from M_0 monomers with: $p = 0$ (red/bottom), $p = 1$ (green/middle), and $p = 2$ (blue/top). Lines are guides to the eye.

Results on θ in Fig. 4 of the main text, Fig. S2, and Fig. S3 were obtained with tubules starting with protofilaments twisted according to Eq. (1) of the main text. However, if the starting state has straight protofilaments, then the pitch of tubules can change, especially when $A_V > A_L$. An example is shown in Fig. S4 for a prebuilt 13_2 tubule of M_0 monomers. Here the starting tubule has straight protofilaments and $A_V = 4.8 > A_L = 3.0$. The tubule quickly transforms into a hybrid structure of 13_0, 13_1, and 13_2 tubules. However, if we ran the simulation at $A_L > A_V$ with the same starting configuration where protofilaments are straight, then the tubule stays at 13_2, but ends up with twisted protofilaments (see Fig. 2 of the main text for the case $A_L = 4.2 > A_V = 2.6$), of which the twist angle is

consistent with Eq. (1) of the main text. The example in Fig. S1 is for a tubule with $p = 3$ under $A_L = 4.2 > A_V = 2.6$. In that case the same final state with twisted protofilaments is achieved even by tubules starting with straight protofilaments, in contrast to the case $A_V > A_L$. However, these tubules are still meta-stable, though when $A_L > A_V$ the depths of the local minima are increased and their meta-stability is enhanced compared with the $A_V > A_L$ case.

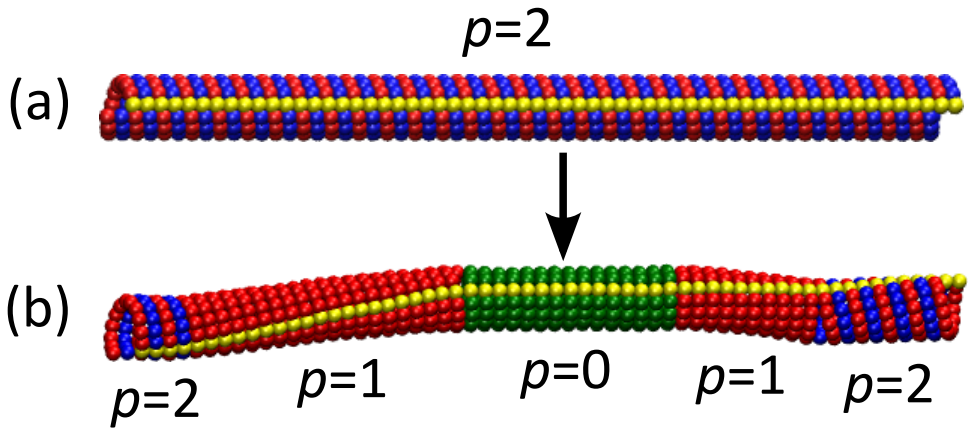

FIG. S4. (a) A pre-built 13_2 tubule of M_0 monomers that contains straight protofilaments. (b) At $A_V = 4.8 > A_L = 3.0$, the tubule in (a) evolves into a state with multiple pitches ($p = 0$, 1, and 2) and the protofilaments are twisted in portions with $p \neq 0$.

Figure S5 helps understand why a larger A_V is needed to initiate the self-assembly of lock-and-key monomers. Here the total potential energy, which is the sum of the repulsions between the gray core sites on two monomers and the attractions between the colored attractive sites (see the Methods section of the main text for more details on the wedge-wedge interactions), is plotted as a function of the separation of wedges that bind at their vertical surfaces. The two wedges are aligned vertically and the interaction energy is calculated as a function of separation. The zero separation corresponds to the state in which the two pairs of vertical binding sites (the sites with the cyan and green color) of two monomers overlap. Because of the repulsion between the gray core sites, the minimum of the potential energy occurs at a positive separation, which is around 0.1σ for the monomers without the lock-and-key configuration. However, for the lock-and-key monomers (see Fig. 1 of the main text for the geometry), the location of the potential minimum shifts to a larger separation (about 0.4σ for the lock-and-key monomers studied in this paper). The underlying reason

is as follows. First, the gray core sites of two lock-and-key monomers start to interact at a larger separation compared with the case without lock-and-key and the interactions are purely repulsive. Then at a given separation the total repulsion between two lock-and-key monomers is always stronger than that between two monomers without lock-and-key, while the total attraction between monomers is the same in the two cases at the same separation. As a consequence, at a given A_V the depth of the potential well of two vertically bound monomers is more shallow for the lock-and-key monomers and the location of its minimum moves to a more positive separation, which is clearly seen from the comparison at $A_V = 3.9$ in Fig. S5. To compensate for this reduction, a larger A_V is needed for the lock-and-key monomers to achieve the same total attraction when two wedges bind vertically. For example, the well depth of the vertical binding of two M_0^{LK} monomers at $A_V = 6.6$ is close to that of two M_0 monomers at $A_V = 3.9$, as shown in Fig. S5. We also find that when the well depth is similar, the curvature of the potential energy around its minimum becomes larger after the introduction of the lock-and-key vertical binding mechanism, which indicates that the potential becomes stiffer and the fluctuations in the vertical bonds are reduced.

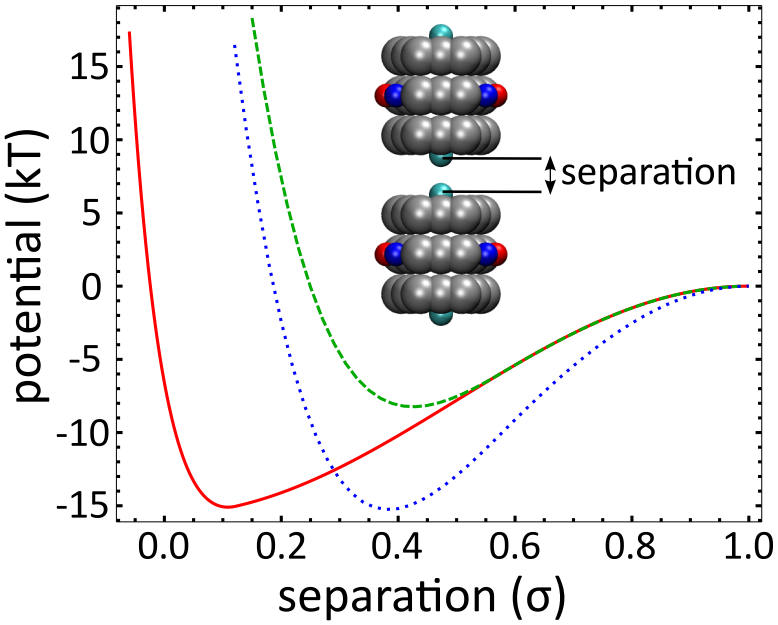

FIG. S5. The potential energy as a function of separation for two monomers binding vertically. Three curves are for two M_0 monomers (inset picture) at $A_V = 3.9$ (red solid line), two M_0^{LK} monomers at $A_V = 3.9$ (green dashed line) and $A_V = 6.6$ (blue dotted line).

Tables I and II summarize all results from assembly simulations starting with free

monomers. As noted in the main text, N_p stands for tubules containing N protofilaments organized with pitch p. Tubules with $p = c$ are shown in bold, where c is the chirality of monomers. The mismatch between p and c frequently occurs for monomers without lock-and-key vertical binding mechanism, as shown in Table I. However, the mismatch can be reduced or even suppressed using monomers with vertical lock-and-key binding, especially when $A_V > A_L$ as shown in Table II. In general, for lock-and-key monomers with $0 \leq c \leq 2$, N_p tubules with $p = c$ dominate when $A_V > A_L$, while N_p tubules with $p = c \pm 1$ dominate when $A_L > A_V$. For M_3^{LK} monomers, N_3 tubules are only found when $A_V > A_L$. For M_3 monomers, tubules with $p = 2$ are the most frequently assembled structures, no matter $A_V > A_L$ or $A_L > A_V$.

A_L	A_V	M_0	M_1	M_2	M_3
3.0	3.9	**11_0, 12_0,** 11_1, 12_1	**11_1, 12_1,** 11_2	**11_2, 12_2**	11_2
4.2	2.6	12_1, 11_2, 12_2	12_0, **12_1,** 11_2	12_0, 13_0, 11_1, 12_1, **12_2, 13_2**	12_1, 11_2, 12_2, **12_3**

TABLE I. Tubule formation by M_c monomers

A_L	A_V	M_0^{LK}	M_1^{LK}	M_2^{LK}	M_3^{LK}
3.0	6.3	**11_0, 12_0**	**11_1, 12_1**	**11_2, 12_2**	11_2, 12_2, **11_3, 15_3**
3.0	6.0	No assembly	**11_1, 12_1**	**11_2, 12_2**	11_2, 12_2
3.3	6.3	Clusters	12_0, **11_1**	**11_2**	11_2, **13_3**
3.3	6.0	**11_0, 12_0,** 11_1, 12_1	14_0, **11_1, 12_1**	12_1, **11_2, 12_2**	11_2, 12_2, **12_3**
3.3	5.7	No assembly	**12_1**	11_1, **11_2, 12_2, 13_2**	11_2, 12_2, 13_2, **11_3**
3.6	6.0	**12_0,** 12_1	**12_1**	13_1, **11_2, 12_2**	13_2, **12_3, 14_3**, 13_4
3.6	5.7	**11_0, 12_0**	**11_1, 12_1**	11_1, 12_1, **12_2**	12_1, 11_2, 12_2, 13_2
3.6	5.4	**12_0,** 12_1	**11_1, 12_1**	11_1, **11_2, 12_2**	12_2, **11_3**
3.9	5.1	**12_0**, 12_1	12_0, **11_1, 12_1, 13_1**, 11_2	12_1, **12_2, 13_2**	12_1, 12_2, **12_3**
4.4	4.2	**12_0**, 12_1, 13_1	12_0, 14_0, **11_1, 12_1, 13_1**	12_0, 13_0, 12_1, 13_1, **12_2,** 11_3	11_1, 12_1, 11_2, 13_2
4.4	3.9	**13_0**, 13_1	12_0, **12_1, 13_1**	12_0, 11_1, 13_1, **11_2, 12_2**	11_0, 12_0, 12_1
4.8	3.6	**13_0**, 12_1	12_0, 13_0, 14_0, **12_1**, 12_2	12_0, 13_0, 14_0, 12_1, 13_1, **12_2**	11_0, 12_0, 11_1, 12_1, 13_1

TABLE II. Tubule formation by M_c^{LK} monomers.